

Generative Latent Coding for Ultra-Low Bitrate Image and Video Compression

Linfeng Qi[✉], Zhaoyang Jia[✉], Jiahao Li[✉], Bin Li[✉], *Member, IEEE*, Houqiang Li[✉], *Fellow, IEEE*, Yan Lu[✉], *Member, IEEE*

Abstract—Most existing approaches for image and video compression perform transform coding in the pixel space to reduce redundancy. However, due to the misalignment between the pixel-space distortion and human perception, such schemes often face the difficulties in achieving both high-realism and high-fidelity at ultra-low bitrate. To solve this problem, we propose Generative Latent Coding (GLC) models for image and video compression, termed GLC-image and GLC-Video. The transform coding of GLC is conducted in the latent space of a generative vector-quantized variational auto-encoder (VQ-VAE). Compared to the pixel-space, such a latent space offers greater sparsity, richer semantics and better alignment with human perception, and show its advantages in achieving high-realism and high-fidelity compression. To further enhance performance, we improve the hyper prior by introducing a spatial categorical hyper module in GLC-image and a spatio-temporal categorical hyper module in GLC-video. Additionally, the code-prediction-based loss function is proposed to enhance the semantic consistency. Experiments demonstrate that our scheme shows high visual quality at ultra-low bitrate for both image and video compression. For image compression, GLC-image achieves an impressive bitrate of less than 0.04 bpp, achieving the same FID as previous SOTA model MS-ILLM while using 45% fewer bitrate on the CLIC 2020 test set. For video compression, GLC-video achieves 65.3% bitrate saving over PLVC in terms of DISTs.

Index Terms—Image compression, video compression, latent domain

I. INTRODUCTION

IMAGE and video compression are crucial in addressing the massive amount of digital visual data that must be stored and transmitted. Most existing approaches, including the traditional codecs [1], [2] and the emerging learned based codecs [3]–[11], perform transform coding in the pixel-space [12] to reduce redundancy. Specifically, these paradigms transform the pixels of the input image or video frame into compact representations, which are then encoded into bitstreams with fewer bits.

However, we observe a common inherent limitation in these methods: the pixel-space distortion is not always consistent with human perception, especially at low bitrates. Human perception prioritizes semantic consistency and texture realism,

Linfeng Qi, Zhaoyang Jia and Houqiang Li are with MoE Key Laboratory of Brain-inspired Intelligent Perception and Cognition, University of Science and Technology of China (e-mail: qlf324@mail.ustc.edu.cn; jzy_ustc@mail.ustc.edu.cn; lihq@ustc.edu.cn).

Jiahao Li, Bin Li, and Yan Lu are with Microsoft Research Asia, Beijing 100080, China (e-mail: li.jiahao@microsoft.com; libin@microsoft.com; yanlu@microsoft.com).

This work was done when Linfeng Qi and Zhaoyang Jia were interns at Microsoft Research Asia.

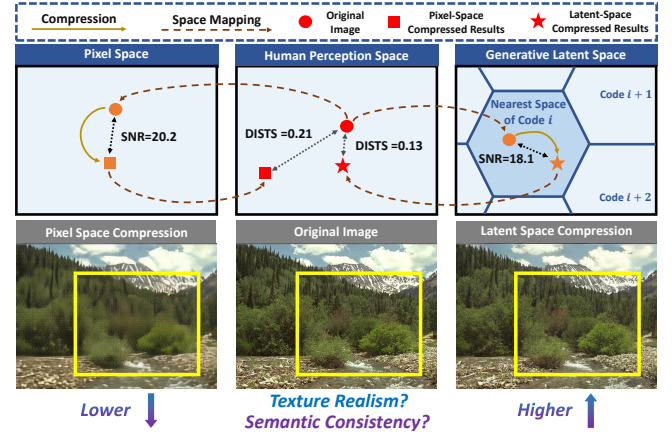


Fig. 1. For ultra-low bitrates, the generative latent space of VQ-VAE provides a better alignment with human perception than the pixel space. At comparable distortion levels, latent-space compression yields reconstructions with superior perceptual quality compared to the pixel-space generative codec MS-ILLM [13], as measured by signal-to-noise ratio (SNR). The perceptual enhancement is quantified using the DISTs metric [16].

which are difficult to be adequately captured using only a pixel-space transform module. As shown in the left of Fig. 1, MS-ILLM [13], previous SOTA pixel-space generative image codec, struggles to guarantee visual quality at low bitrate, even though it is equipped with the perceptual supervision [14] and adversarial supervision [15] within the pixel space.

To address this limitation, we propose **Generative Latent Coding** paradigm for image compression (**GLC-image**) and video compression (**GLC-video**). In our method, input images or video frames are firstly encoded into a generative latent space aligned with human perception, followed by transform coding on the encoded latents to facilitate compression. Specifically, we utilize a generative vector-quantized variational auto-encoder (VQ-VAE) [17], [18] to learn a generative latent space, which offers three significant advantages: 1) The discrete codes of VQ-VAE encapsulate semantic visual components [17], allowing our model to prioritize compressing semantic content, thereby achieving improved visual quality at ultra-low bitrates. 2) Generative VQ-VAE exhibits remarkable generative capabilities [18] for generating high-realism textures. 3) A low-entropy and distortion-robust latent space can be achieved through the discrete variational bottleneck, which is well-suited for compression tasks. These characteristics align our model more closely with human perception and improve visual quality, as illustrated in the right of Fig. 1.

During implementation, two critical problems need to be addressed: 1. *How to effectively compress the generative latents?* 2. *How to supervise the generative latent coding pipeline?* A straightforward approach to compress the latents of VQ-VAE is indices-map coding [19], [20]. However, its ineffective redundancy reduction between indices and the lack of supporting rate-variable coding hinder its practical applicability. To address these limitations, we propose a novel generative-latent-space transform coding approach for GLC-image and GLC-video. The input images or video frames are transformed into latents, and an effective rate-variable structure is implemented to reduce latent redundancy for achieving higher compression ratio. We observe that temporal correlations in video are not restricted to frame pixels but are also preserved within the generative latent space. Leveraging this insight, conditional coding is utilized to compress the current latent using the previously decoded latent as references, effectively reducing temporal redundancy.

In considering effective supervision to guide the training, we draw inspiration from recent advancements in code prediction transformers [19], [21]. We propose a code-prediction-based supervision mechanism, which acts as auxiliary supervision employed solely in the training process and greatly enhances the semantic consistency. To further boost the performance, we improve the hyper module for GLC-image and GLC-video. For GLC-image, we design the spatial categorical hyper module to address the limitations of the factorized hyper module [3]. At ultra-low bitrates, factorized hyper module primarily allocates bits to low-level features. In contrast, our spatial categorical hyper module employs a discrete codebook to capture basic semantic elements for each spatial positions. It brings a better trade-off between preserving essential semantic details and reducing the bit cost of coding hyper-information. For GLC-video, we emphasize the necessity of integrating temporal correlations into the hyper prior to reduce redundancy. We also adopt the concept of the spatial categorical hyper module in GLC-image, utilizing a discrete codebook to model the hyper information. However, independently encoding such categorical hyper information across frames overlooks the inherent temporal correlations, resulting in significant redundancy. Temporal context provides a valuable opportunity to predict regions that are more likely to change within a frame, allowing us to focus on encoding the spatio-temporal information. Moreover, in video sequences, the dynamics of correlated content often follow regular patterns, but the hyper-features with a local receptive field lacks the capability for capturing global and high-level dynamics, such as background motion or camera perspective changes. Therefore, we propose the spatio-temporal categorical hyper module. This module aggregates global semantic dynamics into a compact set of tokens, where each token encapsulates the context of the entire frame rather than a localized region. These tokens act as hyper information, significantly reducing redundancy through capturing global patterns and semantic correlations.

By incorporating these advanced designs, our GLC-image and GLC-video models deliver outstanding performance in image and video compression tasks. On the CLIC 2020 test

set [22], GLC-image achieves a remarkable bitrate of less than 0.04 bpp while maintaining high visual quality, demonstrating a 45% bit savings compared to MS-ILLM [13] at an equivalent FID. In video compression, GLC-video achieves significantly lower bitrates (down to 0.01 bpp) on benchmark video datasets compared to previous generative video codecs such as PLVC [23]. GLC-video can produce visually superior reconstructions compared to the advanced neural video codec DCVC-FM [24] and PLVC even with a lower bpp, further highlighting the effectiveness of our proposed approach.

In summary, our main contributions are:

- We propose a novel generative latent coding scheme, performing transform coding to reduce latent redundancy within the generative latent space of a VQ-VAE. Our scheme not only supports rate-variable image and video compression, but also results in high-fidelity and realistic reconstructions.
- For GLC-image, we introduce a spatial categorical hyper module to reduce the bit cost of hyper information. For GLC-video, we propose a spatio-temporal categorical hyper module to capture global semantic dynamics to reduce redundancy.
- We propose a code-prediction-based supervision strategy to guide the training and tap the potential of the generative latent coding pipeline.
- GLC-image obtains a 45% bit reduction on CLIC2020 with the same FID as the previous advanced method MS-ILLM, and GLC-video provides a 65.3% bitrate saving over PLVC in terms of DISTS on benchmark video datasets, demonstrating the effectiveness of our approach.

This work is built upon our preliminary conference paper [25], with notable enhancements summarized as follows: 1. Leveraging the success of GLC-image and the insight that temporal correlations remain significant in the latent space, we extend the generative latent coding approach to video compression, introducing the GLC-video framework for achieving ultra-low bitrate video compression. 2. To address temporal redundancy, we design a conditional transform coding module that compresses the current latent by utilizing the previously decoded latent as temporal context, thereby improving coding efficiency. 3. Recognizing the temporal redundancy and global motion patterns inherent in hyper information across video frames, we propose a spatio-temporal categorical hyper module. This module predicts regions of change using temporal context and captures global semantic dynamics, enabling more efficient encoding and improved compression performance. 4. We incorporate more recent methods, such as DiffEIC [26], for comprehensive comparisons with GLC-image on benchmark datasets. Extensive experiments and analyses are conducted to evaluate the proposed GLC-video framework, further highlighting the advantages of our generative latent coding.

II. RELATED WORK

A. Learned Image Compression

Learned image compression has seen rapid advancements in recent years. Ballé et al. [12] proposed utilizing neural networks for pixel-space transform coding. They introduced

transform modules to convert images into compact representations for entropy coding. Following this, significant advancements have been made: some studies focus on improving the probability model [3], [4], [12], [27], [28] to achieve more accurate estimation, while others enhance network structures [4], [7], refine optimization algorithms [29] or explore rate-variable coding [6], [30]. These works improve both compression performance and practical applicability.

A critical challenge in modern image compression lies in improving the perceptual quality of reconstructed images. Agustsson et al. [31] introduced the concept of *generative compression*, which focuses on compressing essential image features and generating distorted details using generative adversarial networks (GANs). Building on this concept, subsequent works [32], [33] explored extracting image sketches and latent codes to maintain geometric consistency. However, while these approaches produce visually appealing results, they often deviate significantly from the input, failing to ensure semantic consistency in the reconstructions.

To achieve high-fidelity generative compression, Mentzer et al. [34] explored advanced network structures and generative adversarial loss to improve the fidelity of the reconstructions. Subsequent methods have made notable advancements, including enhancing the transform coding [35], generative post-processing [36] and strategies to control the trade-off between fidelity and realism [37], [38]. MS-ILLM [13] introduced a non-binary discriminator conditioned on quantized local image representations, significantly improving statistical fidelity of generative compression. Gao et al. [39] proposed an invertible image generation based framework to improve the quality of the restored images for extremely low bitrate compression. Recently, probabilistic diffusion models [40] have drawn increasing attention due to its impressive performance on image generation tasks, with perceptual qualities comparable to GAN based methods while maintaining stable training. Some works use diffusion models for image compression. Emiel et al. [36] employ a denoising diffusion model to enhance the quality of reconstructed images. Perco [41] proposes using iterative diffusion models for decoding, which improves image quality while eliminating dependency on bitrate. DiffEIC [26] leverages the latent of images in the diffusion space as guidance for compression at extremely low bitrates. However, these diffusion-based approaches are hindered by significant computational costs, substantial memory requirements, and high latency due to their complex designs and multi-iteration inference processes. Additionally, they are prone to introducing artifacts or deviations that may compromise fidelity to the original image.

B. Learned Video Compression

Most existing learned video compression methods are designed to optimize traditional metrics like PSNR or MS-SSIM [42]. They can be broadly categorized into two categories: residual coding-based frameworks and conditional coding-based frameworks. The residual coding-based framework [8], [43]–[46] typically compute and compress the residuals. A prediction frame is firstly generated from the previously

decoded frame by aligning with the estimated optical flow. Subsequently, the residual between the prediction frame and the current frame is coded for reconstruction. The conditional coding-based frameworks do not directly use a subtraction operation to reduce redundancy, but generates temporal context from previously decoded frames or buffered features [9], [24], [28], [47]–[50]. Compared to residual coding, conditional coding learns temporal context more flexibly. Recently, there has been a growing interest in generative video compression, which focuses on improving perceptual quality rather than solely prioritizing PSNR. For instance, PLVC [23] incorporates a recurrent model with GAN loss to produce visually appealing reconstructions. Similarly, [51] addresses challenges such as poor reconstruction in newly-emerged regions and checkerboard artifacts caused by deconvolutions and optimization inefficiencies. In contrast to these methods, our scheme achieves high-quality visual reconstruction at significantly lower bitrates by performing transform coding in the generative latent space, effectively capturing semantic and temporal dynamics for perceptually-driven video compression.

C. Latent Space Modeling

The latent space modeling technique has been primarily developed for image generation, which involves modeling the distribution of inputs within the latent space of a neural network. Early contributions by Chen et al. [52] and Oord et al. [17] introduced the use of PixelCNN [53] within the latent space of VAE and VQ-VAE for image generation. Esser et al. [18] advanced this idea by integrating transformers into the VQ-VAE latent space, enabling high-quality generation. More recently, Rombach et al. [54] achieved remarkable results in high-resolution image generation by employing diffusion models to model the latent space of VQ-VAE. These studies highlight the potential of utilizing generative latent spaces, particularly the latent space of VQ-VAE.

The concept of latent space modeling has recently been extended to other tasks. For example, CodeFormer [21] introduced a code prediction transformer that uses distorted latents as input and predicts high-quality VQ-VAE indices for facial restoration. Building on this, Jiang et al. [19] proposed transmitting the predicted indices to facilitate restoration-based facial conferencing. In this work, we explore the latent space modeling for generative image and video compression at ultra-low bitrates. Specifically, we design a transform coding paradigm in the latent space, leveraging its alignment with human perception to deliver superior performance for image and video compression.

III. GENERATIVE LATENT CODING

In this section, we introduce the proposed Generative Latent Coding (GLC) paradigm. Our approach performs transform coding within the generative latent space, which is more aligned human perception than the pixel space. The latent space is constructed using a Generative Latent Auto-Encoder (detailed in Sec.III-A). Notably, our latent-space transform coding supports variable bitrates within a single model, as discussed in Sec.III-B. Additionally, we provide a detailed

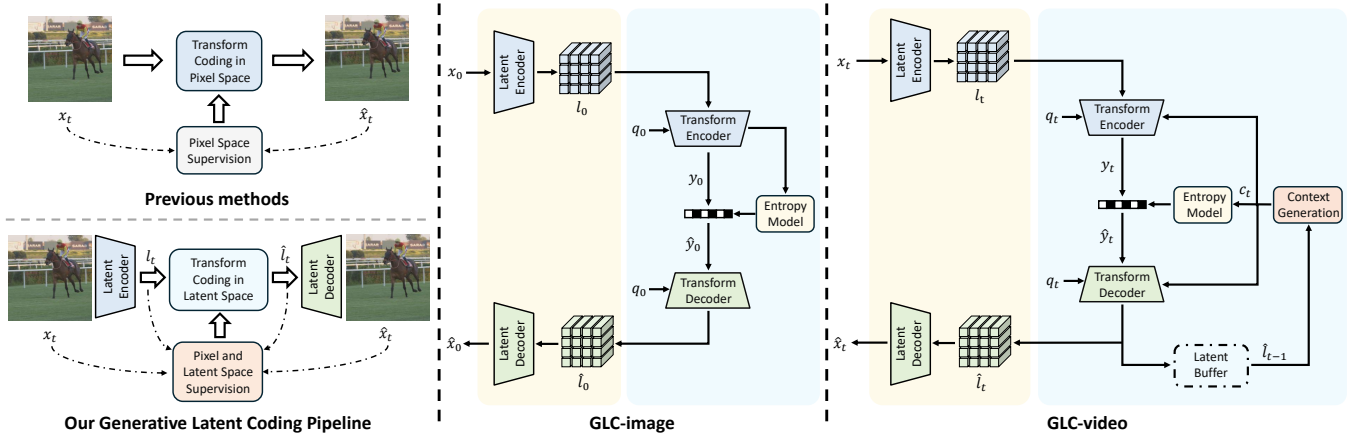


Fig. 2. Left: Comparison with previous methods. Unlike traditional approaches that perform transform coding in the pixel space, our scheme operates in the generative latent space. The generative latent coding pipeline involves three steps: (1) encoding the input into a generative latent space, (2) compressing the latents using transform coding, and (3) decoding the compressed latent to reconstruct the image. Center: Illustration of the proposed GLC-image for image compression. Right: Illustration of the proposed GLC-video for video compression.

discussion on the application of latent-space transform coding for image compression (GLC-Image, Sec.III-C) and video compression (GLC-Video, Sec.III-D).

A. Generative Latent Auto-Encoder

To achieve a latent space aligned with human perception, the GLC pipeline employs a generative VQ-VAE [18] as the latent auto-encoder (E and D). It maps the input image x_t or video frame x_t into visual semantic elements through a discrete codebook B . The codebook size is 16384. Then a generative decoding process is incorporated, ensuring both texture realism and semantic consistency. Additionally, through training with the discrete codebook B as a variational bottleneck, a low-entropy and distortion-robust latent space is achieved, contributing to the compression process.

The proposed GLC-image and GLC-video share the same structure for the generative latent auto-encoder to ensure the consistency of the latent space, and can be uniformly presented (in the left of Fig. 2). The input images or video frames are firstly encoded into the latents using the latent encoder. The latents are then processed by the transform coding, which comprises encoding, scalar-quantization and decoding. Finally, the latent decoder takes the decoded latents as input and generates the reconstructed images or video frames. The overall process can be formulated as follows:

$$\begin{aligned} l_t &= E(x_t), \quad y_t = g_a(l_t, c_t) \\ \hat{y}_t &= Q(y_t) \\ \hat{l}_t &= g_s(\hat{y}_t, c_t), \quad \hat{x}_t = D(\hat{l}_t) \end{aligned} \quad (1)$$

Here, E and D denote the latent encoder and decoder, respectively; g_a and g_s represent the analysis transform (implemented using the transform encoder) and the synthesis transform (implemented using the transform decoder), respectively; x_t , l_t , and y_t correspond to the input image/video frame, the latent, and the code used for entropy coding, respectively; $\hat{\cdot}$ indicates the corresponding reconstruction; t indicates the time step, and c_t denotes the temporal context (for image compression, $t = 0$ and c_t is not applicable); and Q stands for scalar quantization.

B. Rate-Variable Latent Transformation

A straightforward approach to compressing latents l_t is the VQ-indices-map coding [19], [20] (Fig. 3b). These methods reduce the bit cost of individual feature vectors by encoding them into discrete VQ indices, but they overlook the correlations between different feature vectors, consequently resulting in insufficient redundancy reduction and higher bit cost. To address these limitations, our proposed GLC-image and GLC-video frameworks replace the vector-quantization step with a transform coding module, as depicted in Fig.2. The transform coding module processes latents through advanced network structures, converting them into more compact and efficient forms while preserving essential information, thus effectively reducing redundancy. Additionally, for video compression task, transform coding facilitates the modeling of inter-frame correlations by flexibly incorporating the temporal context from the previously decoded latents.

An additional advantage of transform coding over VQ-indices-map coding is its inherent support for rate-variable compression, which is crucial for practical image and video codecs. VQ-indices-map coding is constrained by the limited modeling capacity of its codebook, which can only represent one specified distribution. However, different bitrate levels naturally require the modeling of different distributions. By contrast, transform coding maps the latents into a unified Gaussian distribution, with the rate variability achieved through adjustments to the Gaussian parameters, such as the mean and scale. In the proposed GLC pipeline, we incorporate a scaling factor q_t into the transform coding process, following the strategies employed in advanced variable-bitrate neural codecs [24], [28], [55]. Users can adjust the scaling factor to control the bitrate within a single model, eliminating the need to switch between multiple models.

C. Latent-space Transform Coding for GLC-image

In this section, we detail the design of the latent-space transform coding used in GLC-image. As shown in the center of Fig. 2, the transform coding procedure (Sec. III-C1) consist

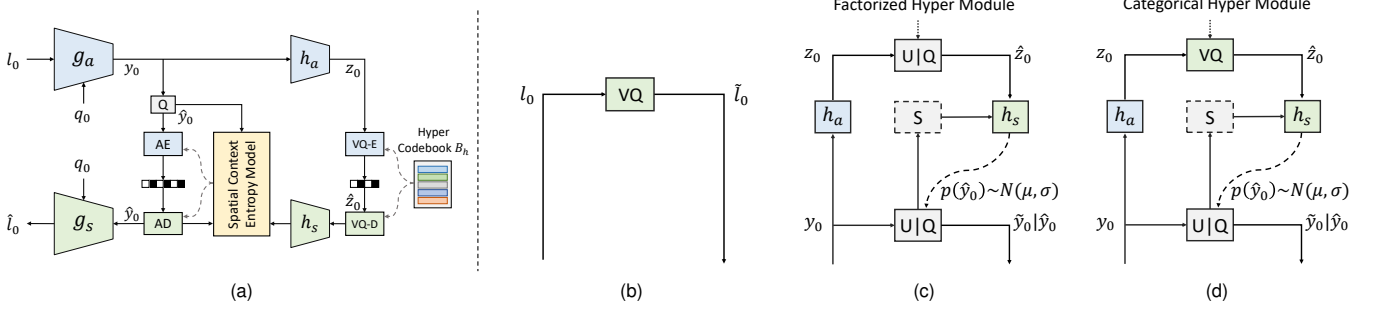


Fig. 3. Illustration of the transform coding in the latent space of GLC-image and comparison with other coding schemes in operational diagrams. (a) The model structure of transform coding module in GLC-image. (b) indices-map coding [19], [20], (c) transform coding with factorized hyper module [3] and (d) proposed transform coding with our spatial categorical hyper module. Here, AE and AD denote arithmetic encoding and decoding, VQ-E and VQ-D refer to VQ-indices-map encoding and decoding, Q represents scalar quantization, U signifies the addition of uniform noise as a differential simulation of Q, and S denotes the spatial context entropy module.

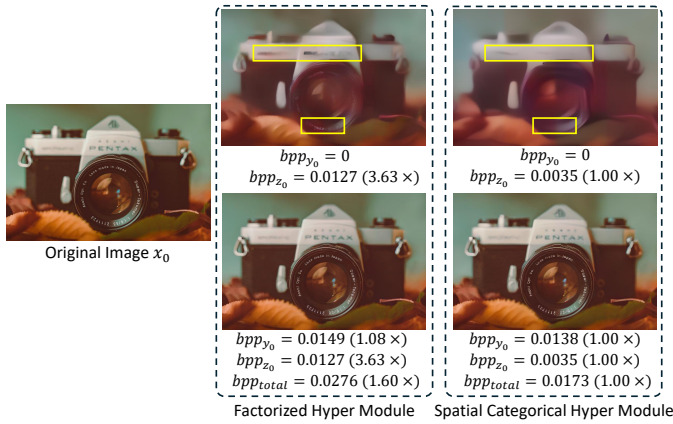


Fig. 4. Visual comparison for the spatial categorical hyper module and factorized hyper module. The bit per pixel (bpp) value for coding y_0 and z_0 , and the bpp multiplier relative to our method are shown. The proposed spatial categorical hyper module encodes essential semantic and structural information with significantly fewer bits while being less susceptible to low-level noise, thereby achieving comparable visual quality and substantially reducing the overall bit cost.

of a transform encoder, a transform decoder, and an entropy model. Considering the characteristics of hyper information at ultra-low bitrates, we further enhance the coding performance by incorporating a spatial categorical hyper module (Sec. III-C2). This module allows for more effective modeling and compression of the hyper information, contributing to the overall efficiency of the system.

1) Transform Coding: The transform encoder and decoder are based on the image codec presented in [28], using cascaded depth-wise convolution blocks for efficient image compression. The main transformations include converting latent l_0 into the code y_0 , as well as the inverse process of converting \hat{y}_0 back into \hat{l}_0 . We configure the number of channels of the latent l_0 and code y_0 as 256. We also incorporate learned scalars q_0^{enc} and q_0^{dec} into the transform encoder and decoder for supporting variable bitrates. The entropy model predicts the probability distribution of the quantized code \hat{y}_0 through the proposed spatial categorical hyper module (Section III-C2) and a spatial context module. The spatial categorical hyper module utilizes a hyper codebook B_h to code the hyper information \hat{z}_0 . During inference, the indices are compressed

using fixed-length coding, where each code index is encoded into $\log_2 N_b$ bits, where N_b represents the size of B_h . For the spatial context module, we adopt the quanttree-partition-based structure from [28], which predicts the probability by leveraging the hyper prior and the previously decoded parts of \hat{y}_0 .

2) Spatial Categorical Hyper Module: Most image compression frameworks employ the factorized hyper module [3] (Fig. 3c) to model the hyper information z_0 . We observe that at ultra-low bitrates, the factorized z_0 predominantly encodes low-level features, such as color and texture. However, it also introduces low-level noise, which not only increase the bit cost of z_0 , but also necessitates extra bits for correction, resulting in a high bit cost, as highlighted by bounding boxes in Fig. 4. To address this issue, we propose a spatial categorical hyper module, as shown in Fig. 3d. It consists of a hyper analysis transform h_a , a hyper synthesis transform h_s , and a hyper codebook B_h . The hyper codebook is employed to store the basic semantic elements. Specifically, the process can be described by the following transformations:

$$z_0 = h_a(y_0), \quad \hat{z}_0 = VQ(z_0, B_h), \quad prior_{z_0} = h_s(\hat{z}_0) \quad (2)$$

where z_0 represent the hyper-codes, \hat{z}_0 refers to the reconstructed hyper-codes, and $VQ(\cdot, B_h)$ denotes vector quantization through nearest lookup in the hyper codebook B_h . This codebook is trained to capture basic semantic elements, bringing a better trade-off between preserving essential semantics and reducing the bit cost of coding hyper-information. As shown in Fig. 4, when only transmitting the hyper information by z_0 , both the factorized hyper module and our spatial categorical hyper module can enable a rough reconstruction of the input x_0 . However, the factorized hyper module primarily focuses on encoding low-level details, resulting in significantly higher bit consumption for z_0 . In contrast, our spatial categorical hyper module avoids encoding low-level noise and focus on capturing high-level semantic information, preserving essential attributes such as shape and rough color. It is shown that, when transmitting both y_0 and z_0 , the model equipped with the spatial categorical hyper module can achieve comparable visual quality but use much fewer bits than the factorized hyper module, showcasing the effectiveness of our proposed method.

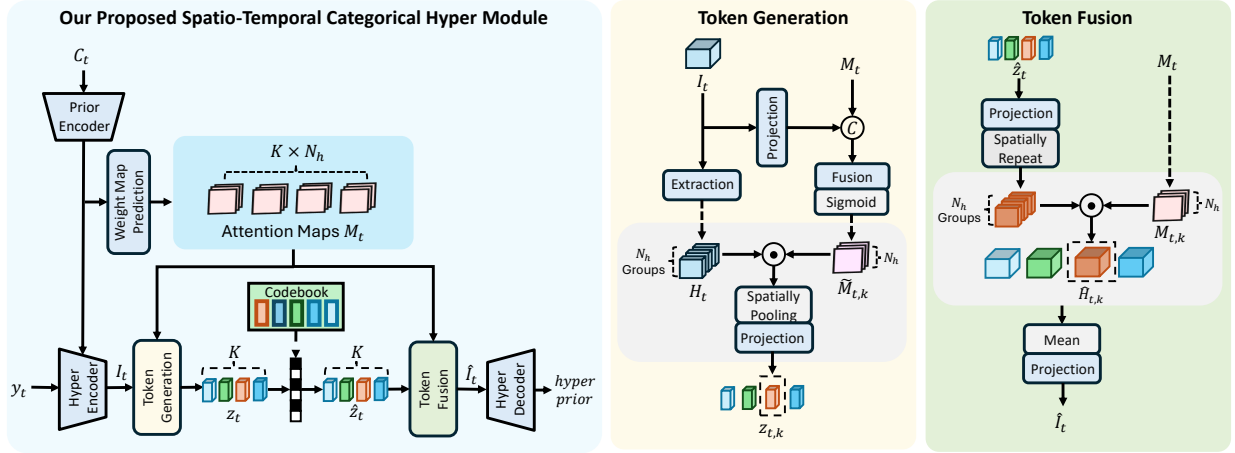


Fig. 5. Our proposed spatio-temporal categorical hyper module in video compression. The token generation and token fusion modules are also illustrated.

D. Latent-space Transform Coding for GLC-video

In the preceding section, we discussed the design of GLC-image, which applies transform coding in the latent space for image compression. In this section, we introduce the latent-space transform coding in our GLC-video for video compression. Recognizing that temporal correlations across frames persist in the latent space, GLC-video converts frames into latents and employs conditional coding to reduce the temporal redundancy. As illustrated on the right side of Fig. 2, besides the generative latent auto-encoder for converting between the latent space and the pixel space, GLC-video employs a conditional latent codec for latent-space transform coding, which facilitates the coding of the current latent l_t using previous decoded latent \hat{l}_{t-1} as temporal conditions. Particularly, the temporal context is also integrated into the spatio-temporal categorical hyper module (Section III-D2), enabling it to capture semantic dynamics as hyper information.

1) *Conditional Transform Coding*: For the model design, we build our conditional latent codec based on the framework presented in [55]. Given that the latent l_t has a resolution of $1/16$ compared to the input x_t , we simplify the context generation process by utilizing cascaded depth-wise convolution blocks. These blocks extract single-scale ($1/16$) features as temporal context, replacing the more complex multi-scale approach in [55]. Similarly, the transform encoder and decoder are streamlined to integrate only single-scale temporal context. The number of channels for the latent l_t , the code y_t , and the temporal context is uniformly set to 256. As conditional information, the temporal context is concatenated with the inputs to both the transform encoder and decoder and further assists in entropy modeling. To enhance the efficiency of entropy modeling, we propose a spatio-temporal categorical hyper module. This module incorporates the temporal context into hyper information and employs a hyper codebook to encode the dynamics across adjacent frames into z_t . Similar to z_0 of GLC-image, z_t is compressed using fixed-length coding. GLC-video is also a rate-variable compression framework, whose bitrate is controlled by the quantization scaler q_t^{enc} and q_t^{dec} generated according to the quantization parameter q_t from the user input.

2) *Spatio-Temporal Categorical Hyper Module*: In Section III-C2, we demonstrated that the proposed spatial categorical hyper module can effectively capture essential spatial semantics using only a few bits for image compression. However, for video compression, it becomes crucial to account for temporal correlations of hyper information and such a module is not sufficiently efficient. Firstly, adjacent frames typically share similar semantics, so independently encoding categorical hyper information can introduce significant redundancy. Secondly, the dynamics of correlated content in a video often follow regular patterns, but the hyper-features with a local receptive field lacks the capability to capture global and high-level dynamics, such as background movement or camera perspective changes. Unlike the dense hyper information required for image compression, the hyper information in video compression is inherently sparse along the temporal dimension and we can encode it into a more compact representation. To address these challenges, we propose a spatio-temporal categorical hyper module in GLC-video. It inherits the idea of the spatial categorical hyper module to utilize a discrete codebook to model semantics. By leveraging temporal context, the proposed hyper module focuses exclusively on capturing changes in semantics between the current and previous frames. Correlated content changes across the entire frame are adaptively aggregated, resulting in a series of tokens z_t . Compared to previous hyper features, our representations benefit from the capability of capturing global semantic dynamics, which enhances its compactness and sparsity, leading to a significantly reduced number of tokens, thereby achieving a higher compression ratio.

Fig. 5 presents the detailed structure of our proposed spatio-temporal categorical hyper module, which operates in three main steps: (1) capturing global semantic dynamics as hyper information into K tokens z_t ; (2) using a hyper codebook to quantize z_t into \hat{z}_t ; and (3) restoring feature maps from \hat{z}_t to serve as hyper priors for entropy coding. Specifically, temporal information is extracted from the temporal context c_t , which assists in extracting the dynamic information as hyper-information from y_t . For each token, N_h attention maps are predicted to indicate the regions that the token emphasizes, resulting in a total of $K \times N_h$ maps, which are subsequently

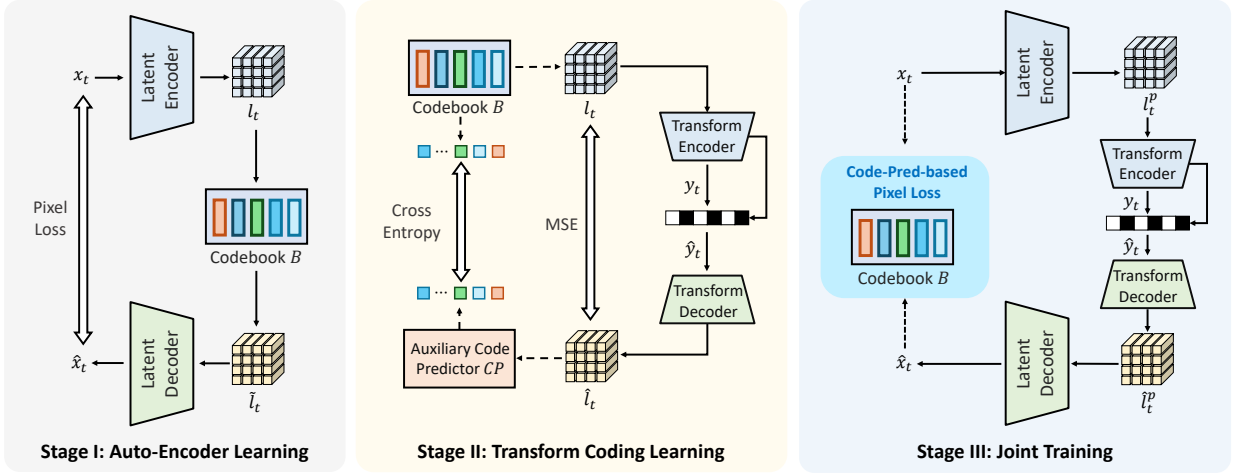


Fig. 6. The progressive training procedure consists of three stages (see Section IV). Stage I: Train the generative VQ-VAE to establish a latent space aligned with human perception. Stage II: Train the transform coding module to effectively compress latents, guided by code-prediction-based latent supervision. Stage III: Jointly fine-tune the entire network using code-prediction-based pixel supervision to further enhance performance.

utilized in the processes of **Token Generation** and **Token Fusion**.

Token Generation. This module selectively encodes the global and high-level dynamics from the entire feature map into the tokens z_t . To ensure comprehensive representation, K tokens are generated using distinct attention maps, each focusing on specific regions to capture diverse information. As shown in the center of Fig. 5, the generation of each token, $z_{t,k}$ ($k \in \{1, \dots, K\}$), is conducted in a group-wise manner. To enhance the attention map by incorporating features of the current time step, the attention maps M_t are fused with the hyper information I_t , yielding refined attention maps $\tilde{M}_{t,k}$ for the k -th token. Features extracted from the hyper information I_t , denoted as H_t , are divided into N_h groups to reduce the computation complexity of the subsequent operations. Next, weighted pooling is applied to facilitate $z_{t,k}$ to selectively encoding hyper information: H_t is firstly multiplied by $\tilde{M}_{t,k}$, (where channels within each group share the same attention map) to emphasize semantic dynamics, followed by global average pooling. Finally, the resulting output is projected onto the token $z_{t,k}$, which will then be coded with the codebook.

Token Fusion. The reconstructed tokens \hat{z}_t encapsulate global and high-level dynamics. To restore spatial-aware information from \hat{z}_t , the token fusion process serves as an approximate inversion of Token Generation, as illustrated on the right side of Fig. 5. To construct the initial feature maps, we project \hat{z}_t through a linear layer, followed by a spatial repetition process. To reintroduce the spatial information, we use the predicted attention maps as guidance. Specifically, element-wise multiplication between the k -th feature map and the corresponding attention map $M_{t,k}$ is conducted in a group-wise manner. Each attention map is shared among the channels within the corresponding channel group. Finally, to fuse distinct information of the K feature maps, we aggregate them by computing their average values, and the output is refined using convolutional layers to synthesize the spatially-aware hyper information \hat{I}_t . This restored hyper information is then fed into the hyper decoder to generate the hyper prior,

which assists entropy coding.

IV. PROGRESSIVE TRAINING OF GLC

In this section, we detail a progressive training strategy designed to fully leverage the potential of our generative latent coding pipeline, as illustrated in Fig. 6. This strategy is structured into three distinct stages, and each stage employs customized loss functions to guide the training of different components, ensuring that each component of the model contributes effectively to the overall performance: 1. Stage I: Auto-Encoder Learning (Section IV-A), where the focus is on learning a perceptually aligned latent space to ensure high-quality reconstructions. 2. Stage II: Transform Coding Learning (Section IV-B), which involves training the model to perform efficient transform coding on the learned latent space, targeting ultra-low bitrates. 3. Stage III: Joint Training (Section IV-C), which finetunes the entire network to optimize the overall compression performance.

A. Stage I : Auto-Encoder Learning

The primary goal of this stage is to establish a latent space that aligns with human perception, improving the quality of reconstructed images. We train a generative VQ-VAE as the initialization for the latent encoder E and decoder D . To promote sparsity in the latent space, an auxiliary codebook B is introduced for nearest vector-quantization, transforming the latent l_t into \tilde{l}_t . The training objective \mathcal{L}_{AE} combines multiple loss functions: reconstruction loss, perceptual loss [14], adversarial loss [15], and codebook loss [17]:

$$\begin{aligned} \mathcal{L}_{AE} = & \|x_t - \hat{x}_t\| + \mathcal{L}_{lips}(x_t, \hat{x}_t) + w_{adv} \cdot \mathcal{L}_{adv}(x_t, \hat{x}_t) \\ & + \underbrace{\|\text{sg}(l_t) - \tilde{l}_t\| + \beta \cdot \|\text{sg}(\tilde{l}_t) - l_t\|}_{\mathcal{L}_{codebook}} \end{aligned} \quad (3)$$

Here, \mathcal{L}_{lips} represents the perceptual loss computed using LPIPS, which leverages VGG features [56] to measure perceptual similarity. Additionally, $w_{adv} = 0.8$ is the weight assigned

to the adaptive Patch-GAN adversarial loss [18], promoting realism in the reconstructed images. $\text{sg}(\cdot)$ denotes the stop-gradient operator and $\beta = 0.25$ is utilized to control the update rates of the E and B .

B. Stage II : Transform Coding Learning

With the perceptually aligned latent space established, the next step involves training the transform coding module for compressing latents at ultra-low bitrates. During this stage, the auto-encoder (E and D) is fixed. To improve semantic consistency, we introduce an auxiliary code predictor (CP), which consists of 9 transformer layers [57] and a linear classifier. It necessitates the latent to possess the capability to predict the correct VQ-indices.

As shown in Fig. 6, the latent l_t is encoded into VQ-indices by $V_{l_t} = VQ(l_t, C)$. Subsequently, these indices are predicted by $\hat{V}_{l_t} = CP(\hat{l}_t)$. The code-prediction-based loss can be formulated by

$$\mathcal{D}_{code}(l_t, \hat{l}_t) = \alpha \cdot CE(V_{l_t}, \hat{V}_{l_t}) + ||l_t - \hat{l}_t||_2^2 \quad (4)$$

where CE denotes the cross entropy loss and α is set to 0.5 by default. The transform coding module is supervised with the following rate-distortion objective:

$$\mathcal{L}_{TC} = \mathbf{E}_{x_t \sim p_{X_t}} [\mathcal{R}(\hat{y}_t) + \lambda \cdot \mathcal{D}_{code}(l_t, \hat{l}_t)] \quad (5)$$

where \mathcal{R} represents the estimated rate, and λ is used to control the trade-off between rate and distortion. It is worth noting that the hyper codebook B_h in the spatial categorical hyper module requires to be trained by the codebook loss (as formulated in Equation 3). For conciseness, it is omitted in the loss functions of stage II and stage III.

C. Stage III : Joint Training

In the final stage, the entire network undergoes joint fine-tuning to further improve compression performance. The code-prediction-based latent supervision is extended into the pixel space and the training procedure is guided with the pixel space supervision. As illustrated in Fig. 6, the encoder E_{VQ} , which is trained from stage I, is utilized to encode x_t and \hat{x}_t into latent space by $\hat{l}_t^p = E_{VQ}(\hat{x}_t)$ and $l_t^p = E_{VQ}(x_t)$. And the code-prediction-based pixel supervision can be calculated by $\mathcal{D}_{code}(l_t^p, \hat{l}_t^p)$ in the same formulation with Equation 4. Here E_{VQ} is used because it can map the input to a compatible latent space with the codebook B for code prediction. The pixel space supervision can be described as :

$$\begin{aligned} \mathcal{D}_{JT} = & ||x_t - \hat{x}_t|| + \mathcal{L}_{lpips}(x_t, \hat{x}_t) \\ & + \lambda_{adv} \cdot \mathcal{L}_{adv}(x_t, \hat{x}_t) + \lambda_{code} \cdot \mathcal{D}_{code}(l_t^p, \hat{l}_t^p) \end{aligned} \quad (6)$$

where we set $\lambda_{code} = 0.05$ by default. The overall objective becomes:

$$\mathcal{L}_{JT} = \mathbf{E}_{x_t \sim p_{X_t}} [\mathcal{R}(\hat{y}_t) + \lambda \cdot \mathcal{D}_{JT}] \quad (7)$$



Fig. 7. A visual example comparing pixel-level metrics (PSNR, MS-SSIM and LPIPS) and image-level metric DISTS.

D. Discussion of Code-Prediction-Based Loss

Recent studies [19], [21] highlight the effectiveness of code-prediction transformers for high-quality reconstructions, which typically feed the predicted latent directly into the decoder for reconstruction. Different from these methods, our approach considers code prediction solely as an auxiliary supervision during training, without incorporating it into the inference process of the compression pipeline.

This design is grounded in the following observation: when a code prediction module is introduced before the decoder, the fine-tuning process in stage III cannot further enhance compression performance. It arises because the codebook becomes a performance bottleneck, restricting the input of the decoder to the vector-quantized latent, which has already been well-trained in stage I. In our approach, this bottleneck is eliminated by utilizing the code prediction solely as auxiliary supervision during training. Specifically, the VQ operation with codebook B is utilized only during training stage I (auto-encoder learning) of progressive training. In the subsequent stages, it serves merely as an auxiliary supervision and no longer strictly constrains the information of l_t . Consequently, in stage II, stage III, and during inference, the codebook B is not required for coding l_t (only the hyper VQ codebook B_h is necessary for the hyper module). It allows more flexible input for the decoder, benefiting the additional fine-tuning. This code-prediction-based supervision can effectively improve the semantic consistency of the reconstructed images. By necessitating the latent to have the ability for predicting the code index, the latent inherently encodes richer semantic information, such as gestures and attributes.

V. EXPERIMENTS

A. Implementation Details

Structure of Latent Auto-Encoder. Considering the generative capability and sparse latent space, we employ the generative VQVAE model [18] as the latent auto-encoder. We adopt the same structure as VQGAN [18], with a latent resolution of $f = 1/16$ of the original input and a codebook size of 16384.

Training details. For GLC-image, we also follow [25] and use OpenImage test set [58] for training, using randomly cropped 256×256 patches. For GLC-video, we follow the strategy adopted by [24], where 256×256 patches are randomly cropped from vimeo dataset [59] for training. Both models are optimized by AdamW [60] with a batch size of 8. For each batch, we train the model with different λ to achieve rate-variable compression ($\lambda \in [0.08, 0.32]$) for GLC-image and

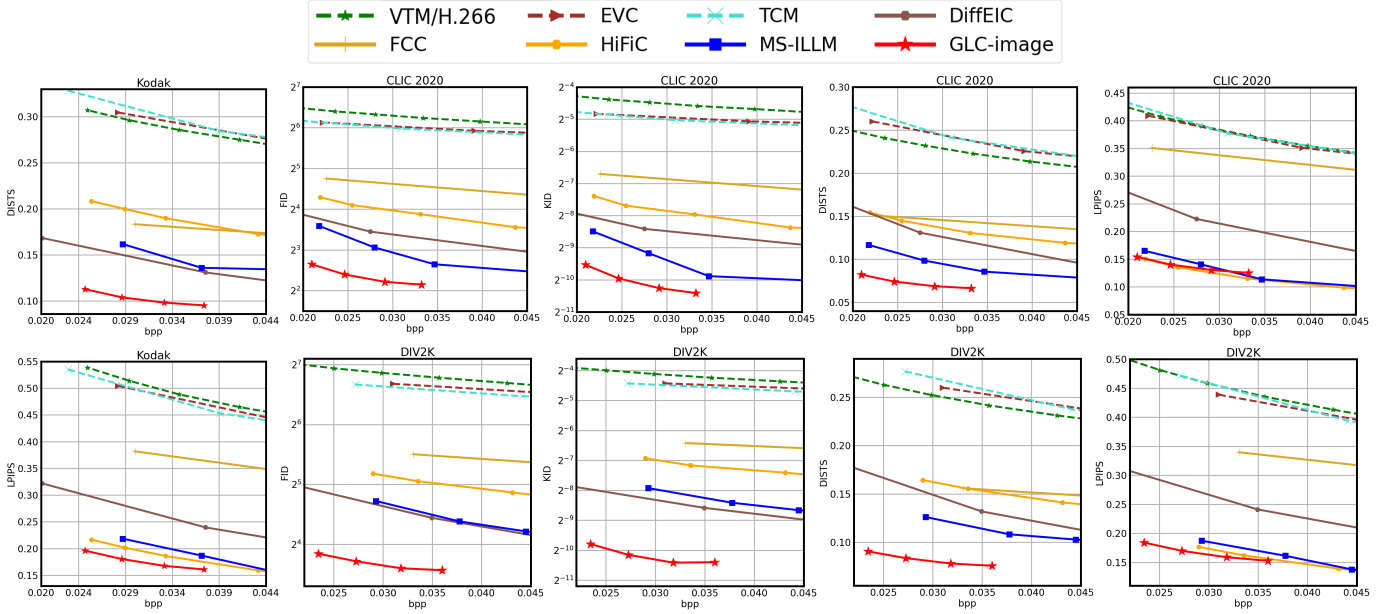


Fig. 8. Rate-Distortion curves for comparing DISTs, FID, KID and LPIPS of the proposed GLC-image and other methods on Kodak, CLIC 2020 test set and DIV2K datasets.

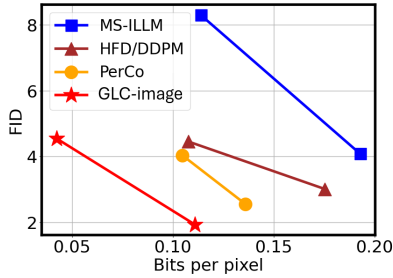


Fig. 9. Comparison with recent methods on MS-COCO 30K dataset.

$\lambda \in [0.12, 1.6]$ for GLC-video).

Evaluation dataset. We evaluate GLC-image on CLIC 2020 test set [22] with original resolution for image compression. We also show the results on Kodak [61], DIV2K [62] and MS-COCO 30K [63]. For evaluating GLC-video, we employ 1080p datasets, including UVG [64], MCL-JCV [65] and HEVC Class B [66].

Evaluation metrics. For image compression, visual quality is evaluated using the reference perceptual metrics DISTs [16] and LPIPS [14], along with the no-reference perceptual metrics FID [67] and KID [68]. For video compression, visual quality is assessed using DISTs and LPIPS. In both image and video compression, bits per pixel (bpp) is used to quantify the bitstream size.

Discussion about Measurements. It is worth noting that the pixel-level distortion metric LPIPS has inherent limitations for assessing visual quality, particularly when evaluating compression methods at ultra-low bitrates, as discussed in [16], [33]. These limitations stem from the fact that LPIPS prioritizes on pixel-level accuracy rather than semantic consistency and texture realism. As illustrated in Fig. 7, the superior result is highlighted in brown. The image on the right is perceptually superior to the one in the middle, despite having lower PSNR,

MS-SSIM, and LPIPS scores. In contrast, the image-level metric DISTs offers a more accurate evaluation of perceptual quality. Consequently, this paper primarily focuses on DISTs, FID, and KID as evaluation metrics, rather than LPIPS.

Computation of FID and KID. For image compression, following established practices in generative image compression methods [13], [34], evaluation is conducted by splitting each image into 256×256 patches. Specifically, an $H \times W$ image is divided into $\lfloor H/256 \rfloor \cdot \lfloor W/256 \rfloor$ patches. The extraction origin is then shifted by 128 pixels in both dimensions to generate an additional set of $(\lfloor H/256 \rfloor - 1) \cdot (\lfloor W/256 \rfloor - 1)$ patches. Consistent with [13], [34], FID and KID are not reported for Kodak [61] due to the limited number of patches (192) derived from its 24 images.

Baseline methods. For image compression, we compare with traditional codec VTM/H.266 [2], neural image codec TCM [7], EVC [6], and generative image codec FCC [37], HiFiC [34], MS-ILLM [13]. As some methods do not release models for ultra-low bitrate, we either retrain or fine-tune their models to suit such low bitrate. In addition, we also compare with recent diffusion based methods [26], [36], [41]. For video compression, we compare against traditional codecs HM/H.266 and H.266/VTM [2], previous advanced neural video codec DCVC-FM [24], and generative video codec PLVC [23]. For each video sequence, we evaluate 96 frames where the intra-period is set to -1.

B. Experiments for Image Compression

In this section, we present the primary results of our GLC-image framework on widely used benchmark datasets and perform ablation studies to validate the effectiveness of each proposed component. For the ablation studies, we evaluate the BD-Rate [69] based on the FID-BPP curve using the CLIC 2020 test set.

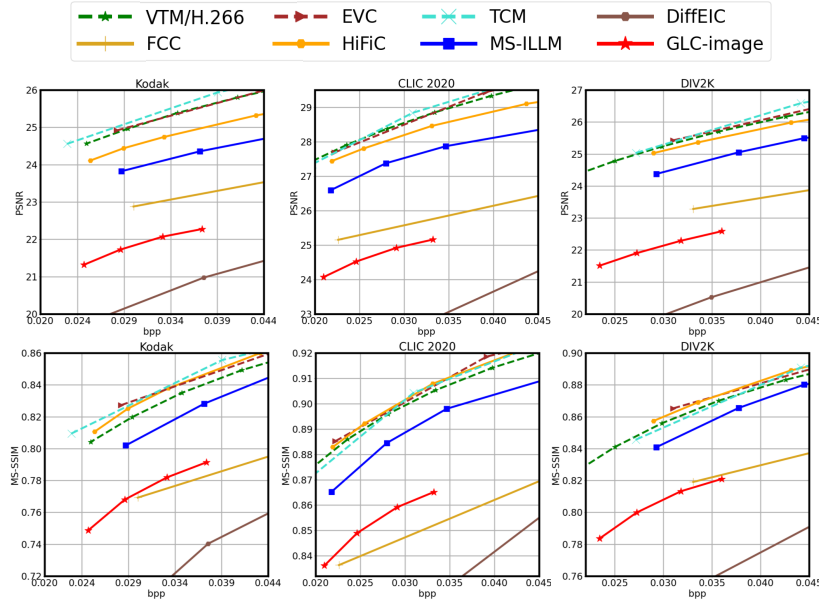


Fig. 10. Rate-Distortion curves for comparing PSNR and MS-SSIM of the proposed GLC-image and other methods on Kodak, CLIC 2020 test set and DIV2K datasets.

Performance Comparisons. Fig. 8 shows the performance of the GLC-image and compared methods at ultra-low bitrate. It is noted that we utilized an 80G NVIDIA A100 Tensor Core GPU, ensuring that DiffEIC [26] had sufficient memory to be tested at the original resolution. On CLIC 2020, GLC-image demonstrates superiority in terms of DISTs, FID and KID than other methods. Specifically, GLC-image saves about 45% bits compared to MS-ILLM while maintaining an equivalent FID. When comparing the pixel-level metric LPIPS, GLC-image also achieves comparable performance with high-fidelity generative codecs such as HiFiC and MS-ILLM. In addition, we compare the proposed GLC-image with recent works HFD [36] and PerCo [41], along with MS-ILLM, on the MS-COCO 30K dataset [63]. Following the methodology of [36], we select the same images as them from the 2014 validation set to generate 256×256 patches. To match the quality range of their models, we further train a codec around 0.12 bpp for comparison (the corresponding latent auto-encoder has $f = \frac{1}{8}$ and $M = 256$). As shown in Fig. 9, our model exhibits significant performance improvement.

Fig. 10 presents the Rate-Distortion (R-D) curves for PSNR and MS-SSIM on GLC-image. While our model underperforms non-generative methods in terms of PSNR and MS-SSIM. This is expected, as it prioritizes perceptual quality enhancement in ultra-low-bitrate scenarios, where generated details may reduce these metrics. Notably, unlike diffusion-based approaches such as DiffEIC [26], our method avoids severe semantic distortions, as demonstrated in Fig. 11.

Visual Comparisons. Fig. 11 illustrates the qualitative comparison results. Existing methods struggle to produce satisfactory reconstructions at ultra-low bitrates, either suffering from blurry artifacts or yielding low-fidelity outputs. For instance, DiffEIC often fails to retain essential semantic details, such as the surging waves in the first example and the texture on the surface in the second example. TCM, HiFiC, and MS-ILLM generate blurry reconstructions, losing crucial details in the

highlighted regions. In contrast, GLC-image delivers visually appealing results, excelling in both realism and fidelity, even at a lower bitrate.

To assess the impact of training stage III (joint training) on latent space sparsity, Fig. 12 shows a t-SNE [70] visualization of latent distributions on the Kodak [61] dataset. Note that vector quantization is not applied to the latents in either stage I or III. These results reveal that VQ-VAE trained by stage I (auto-encoder learning) produces sparser and more clustered latents than VAE. Importantly, the latent encoder in stage III (joint training) preserves this sparsity, despite the absence of vector quantization by codebook B . In our method, vector quantization on l_t is only used during stage I as an information bottleneck. These findings suggest that our model can benefit from the sparser and more structured latent space of VQ-VAE, which contribute to improved coding efficiency and robustness at extremely low bitrates.

Ablation Study on transform coding. A straightforward approach to compress the VQ-VAE latents is indices-map coding [19], [20]. However, it causes 66.2% performance loss compared with transform coding, as shown in Table I. It shows the effectiveness of transform coding on reducing redundancy.

Ablation Study on spatial categorical hyper module. In Section III-C2, we highlight the advantages of employing our spatial categorical hyper module to model z compared to the commonly used factorized based hyper module. Table I further provides a quantitative comparison, demonstrating a significant improvement of 17.7% with this design.

Ablation Study on code-prediction-based supervision. Section IV introduces the use of a code-prediction module as an auxiliary loss during training, instead of during the inference process of the model pipeline as in prior works [19], [21]. As shown in Table II, incorporating the code prediction module directly into the network leads to a drastic 60.7% performance drop. Furthermore, we conducted an additional comparison by removing the code-prediction-based supervi-

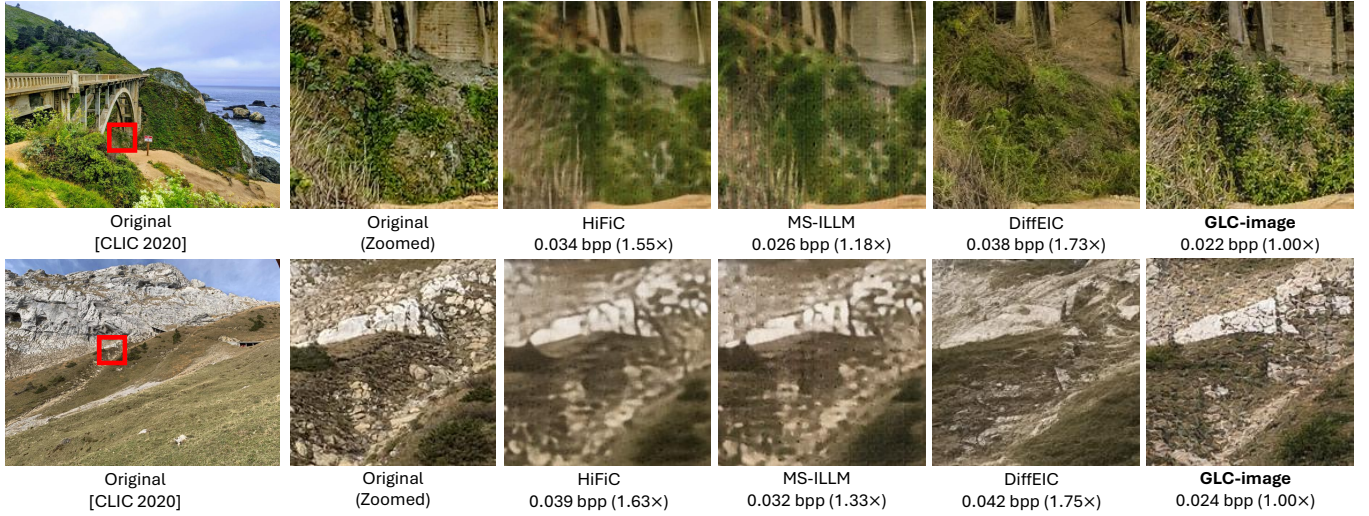


Fig. 11. Qualitative examples for comparing the proposed GLC-image with other methods. For each method, we not only present the bit per pixel (bpp) value for coding the image, but also show the bpp multiplier relative to our method.

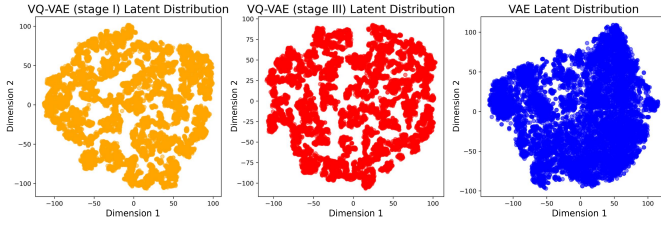


Fig. 12. Visualization by t-SNE for comparing the latent distribution on Kodak [61] dataset.

TABLE I
ABLATION STUDY ON LATENT-SPACE COMPRESSION FOR GLC-IMAGE.

Latent coding scheme	Hyper module	BD-Rate ↓
Indices-map coding	-	66.2%
Transform coding	Factorized based Categorical based	17.7% 0%

sion. The results show that adopting the code-prediction-based supervision yields a 13.1% performance improvement.

Complexity. We conduct the complexity analysis for GLC-image and previous methods using an NVIDIA A100 Tensor Core GPU. As presented in Table III, GLC-image not only show a better Rate-distortion performance measured by BD-Rate with DISTS (68.5% performance improvement), but also can achieve and comparable latency compared to MS-ILLM on Kodak. Table IV presents the runtime and parameter count of GLC-image at the module level, including the latent encoder/decoder and the transform encoder/decoder. The results indicate that the majority of the computational cost is attributed to the latent encoder and decoder, while the transform encoder and decoder are lightweight and efficient.

C. Experiments for Video Compression

In this section, we present the experimental results of our GLC-video framework on benchmark datasets for video

TABLE II
ABLATION STUDY ON THE CODE PREDICTION MODULE.

Code prediction usage	BD-Rate ↓
w/o code pred.	13.1%
code pred. in network	60.7%
code pred. as supervision	0%

TABLE III
COMPLEXITY COMPARISON FOR GLC-IMAGE ON KODAK WITH RESOLUTION OF 512×768 .

Model	Latency (ms) Enc. Dec.	Params	BD-Rate↓
MS-ILLM	41.8 53.5	181 M	0
GLC-image	37.1 58.6	105 M	-68.5%

TABLE IV
MODULE-LEVEL COMPLEXITY COMPARISON FOR GLC-IMAGE ON KODAK WITH RESOLUTION OF 512×768 .

Module	Running time (ms)	Params
Latent encoder	27.3	29.4M
Latent decoder	45.9	42.5M
Transform encoder	0.48	2.4M
Transform decoder	0.48	2.4M

compression. Additionally, we conduct ablation studies to validate the effectiveness of the proposed spatio-temporal categorical hyper module. The performance is evaluated using BD-Rate [69] with respect to DISTS.

Performance Comparisons. In Fig. 13, the Rate-Distortion curves are illustrated for comparing our proposed GLC-video with HM/H.266, VTM/H.266 [2], DCVC-FM [24] and PLVC [23]. As mentioned, DISTS provides a more accurate assessment of visual quality and we mainly focus on this

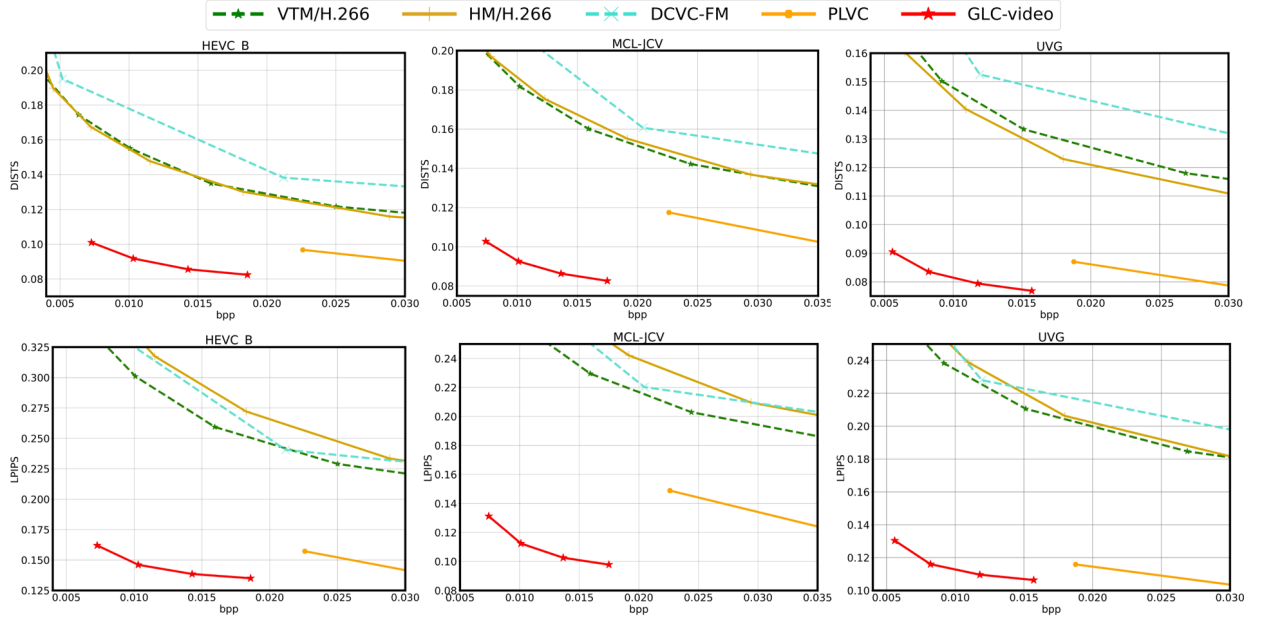


Fig. 13. Rate-Distortion curves for comparing DISTs and LPIPS of GLC-video and other methods on HEVC class B, MCL-JCV, and UVG datasets.

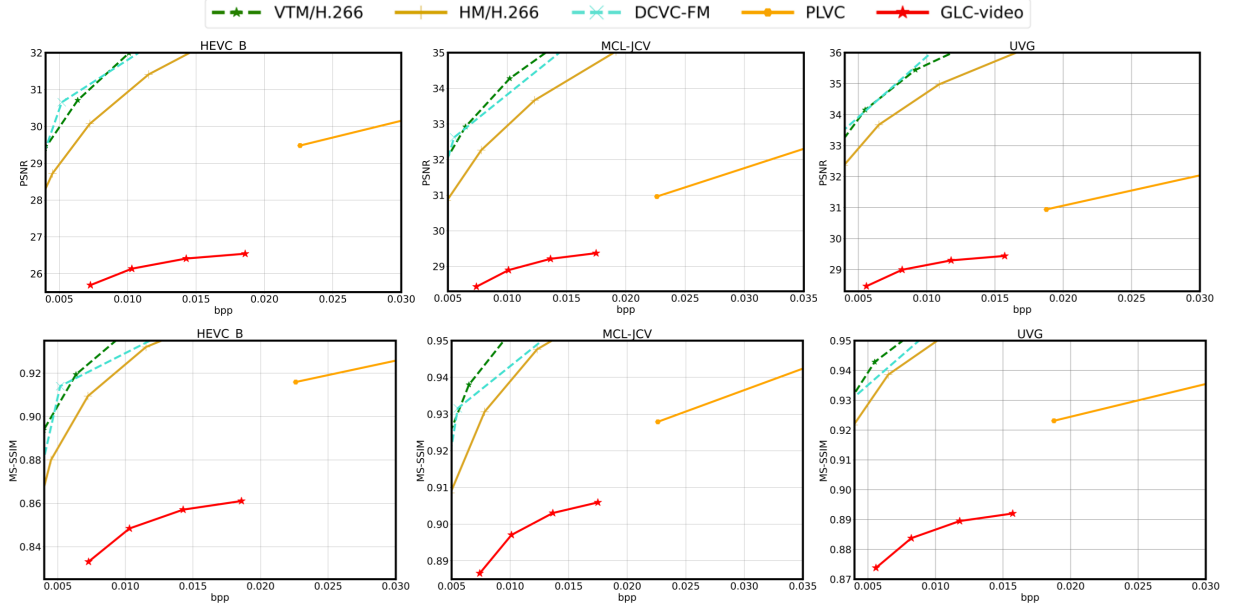


Fig. 14. Rate-Distortion curves for comparing PSNR and MS-SSIM of GLC-video and other methods on HEVC class B, MCL-JCV, and UVG datasets.

metric. Thanks to performing coding in the generative latent space, our proposed GLC-video can work at much lower bitrate than PLVC [23]. Compared with traditional video codec HM/H.266, H.266/VTM, and the previous advanced neural codec DCVC-FM [24], our method provides much better perceptual quality measured by DISTs and LPIPS. When using PLVC as the anchor method, GLC-video provides an average of 65.3% bitrate saving in term of DISTs on these video datasets, demonstrating the effectiveness of our method.

Fig. 14 shows the rate-distortion curves in terms of PSNR and MS-SSIM for GLC-video. Similar to other generative codecs, GLC-video exhibits lower performance than non-generative methods under these distortion-based metrics. However, it is argued that perceptual metrics are more appropriate

for evaluating the visual quality of our generative codec, especially at ultra-low bitrates. Although GLC-video produces reconstructions with lower PSNR and MS-SSIM scores, it can effectively reduce blurry artifacts and generate more visually appealing details (as shown in Fig. 15).

Visual Comparisons. Fig. 15 presents a qualitative comparison of our GLC-video against other methods. At ultra-low bitrates, H.266/VTM, HM/H.266, and DCVC-FM exhibit limited perceptual quality, characterized by noticeable blurry artifacts. While PLVC achieves enhanced perceptual quality through the use of GAN loss, our GLC-video leverages the generative latent space of VQ-VAE, which aligns more closely with human perception. As a result, GLC-video produces more visually appealing reconstructions, even at bitrates lower than

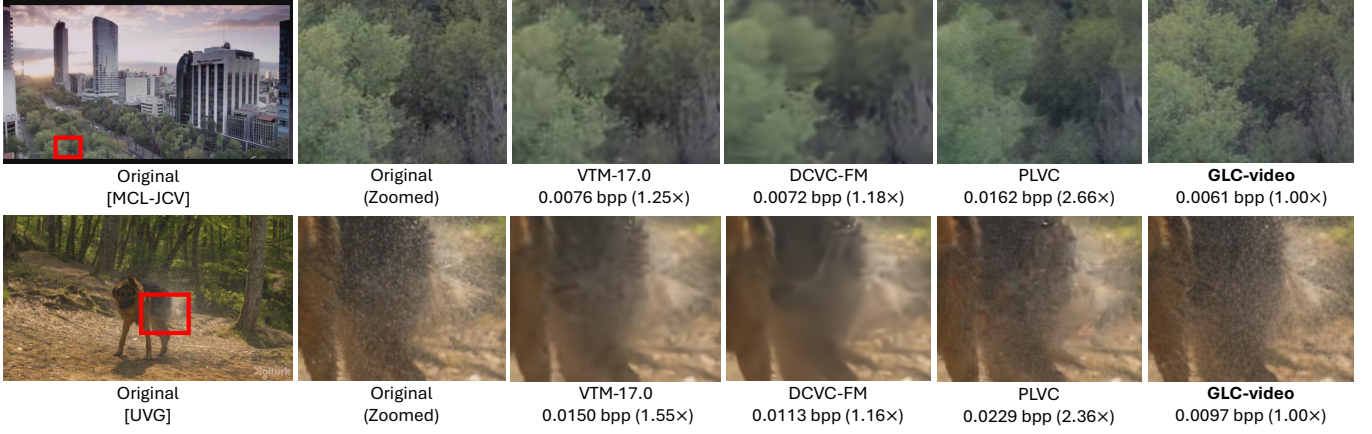


Fig. 15. Qualitative examples for comparing the proposed GLC-video with other methods. For each method, we not only annotate the bit per pixel (bpp) for coding the video sequence, but also show the bpp multiplier relative to our method.

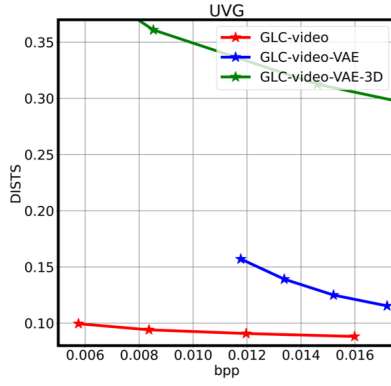


Fig. 16. Ablation study on the latent encoder and decoder of GLC-video on UVG dataset (resized to 720p).



Fig. 17. Visualization for comparing the latent of VQ-VAE and VAE. The feature map of VQ-VAE is more distinct than that of the VAE. Its reconstruction is also sharper, while VAE shows noticeable blurring (even at higher bitrates).

those used by PLVC.

Ablation on the Latent Auto-Encoder. Temporal redundancy can also be reduced by using a 3D VAE to jointly compressing spatial and temporal information. However, a smaller latent dimension does not guarantee a lower bitrate, as the latent may still retain high entropy. Figure 16 shows a comparison of latent auto-encoders for GLC-video on the UVG dataset (downsampled to 720p via bicubic interpolation to save memory). We adopt the 3D VAE from CogVideoX [71] as the latent auto-encoder, denoted as GLC-video-VAE-3D.

TABLE V
ABLATION STUDY ON LATENT-SPACE COMPRESSION FOR GLC-VIDEO.

Latent coding scheme	Hyper module	BD-Rate ↓
w/o conditional coding	Spatial categorical based	214.6%
	Factorized based	20.7%
w/ conditional coding	Spatial categorical based	0%
	Spatio-temporal categorical based	-22.5%

TABLE VI
ABLATION STUDY ON THE TRAINING STRATEGY FOR GLC-VIDEO.

Training strategy	w/o joint training	w/ joint training
BD-Rate ↓	0	-49.8%

TABLE VII
ABLATION STUDY ON THE NUMBER OF TOKENS K OF THE SPATIO-TEMPORAL CATEGORICAL HYPER MODULE OF GLC-VIDEO.

# Tokens	$K = 4$	$K = 8$	$K = 16$	$K = 24$	$K = 32$
BD-Rate ↓	13.0%	-3.9%	-22.5%	-10.1%	-10.0%

For fairness, we also implement GLC-video-VAE, which uses a 2D VAE with a similar parameter size to the VQ-VAE used in GLC-video. GLC-video-VAE-3D performs worse than GLC-video-VAE, mainly due to higher entropy in its latent representation despite lower dimensionality. Although off-the-shelf 3D video tokenizers are still limited, joint spatial-temporal modeling remains a promising direction for further exploration. Moreover, replacing VQ-VAE with a standard VAE results in noticeable performance degradation, primarily because the VQ-VAE produces a sparser latent space. As shown in Fig. 17, VQ-VAE retains semantic information more effectively under ultra-low bitrate settings.

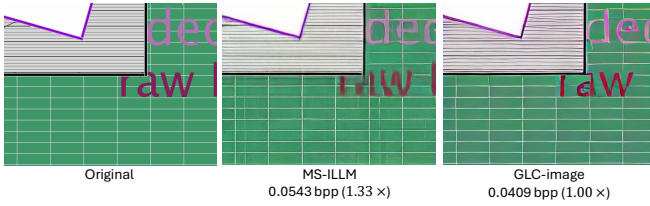


Fig. 18. Visual comparison for GLC-image on a screen image. Discrepancies from the original image are observed in the text region.

Ablation Study on conditinal coding. As shown in Table V, introducing conditional coding significantly improves overall performance. This improvement stems from the fact that compressing the current latent benefits from temporal context extracted from the previously decoded latents, effectively reducing temporal redundancy. During stage II (transform coding learning) and stage III (joint training), feature propagation further enhances the utilization of correlations across multiple frames.

Ablation Study on the Hyper Module. Table V also compares the proposed spatio-temporal categorical hyper module with the factorized based hyper module and the spatial categorical hyper module from GLC-image. The spatial categorical hyper module demonstrates better performance than the factorized based approach, consistent with observations in GLC-image for image compression. Notably, the proposed spatio-temporal categorical hyper module achieves the best performance, providing a 22.5% bitrate saving compared to the spatial categorical hyper module. This improvement can be attributed to the incorporation of temporal context and the effective exploitation of the sparsity along the temporal dimension in hyper-information. By representing z_t more compactly, our method significantly reduces the bitrate.

Ablation Study on the Number of Tokens K . K controls how many tokens are computed as z_t for transmitting the hyper information, thus influencing the capacity of the proposed spatio-temporal categorical hyper module and the corresponding bit cost. Table VII presents a comparison of performance for different values of K . We use the model equipped with the spatial categorical hyper module as the anchor method. A smaller K (e.g., $K = 4$ and $K = 8$) may fail to effectively represent the hyper-information, leading to a performance drop. Conversely, a larger K increases the bit cost for representing the hyper-information and adds complexity to learning the attention maps M_t , thereby increasing training difficulty. The results show that $K = 16$ achieves the best performance, and this value is adopted in our model.

VI. LIMITATIONS

Despite the improvements introduced, GLC-image and GLC-video still encounter several limitations. Although the proposed methods maintain semantic-level consistency and enhance visual quality, they still show limitations in pixel-level metrics such as PSNR, similar to existing generative approaches. GLC-image struggles with accurately reconstructing texts, as evident in the distortions shown in Fig. 18. For GLC-video, several techniques have been adopted to enhance temporal consistency: 1. feature propagation during training

and 2. a two-frame input to the discriminator for Patch-GAN adversarial loss. However, though GLC-video show more stable reconstructions than PLVC [23], it still falls short of the non-generative method DCVC-FM [24] in terms of pixel-level stability. Flickering artifacts can still be observed in some regions under close inspection.

VII. CONCLUSION

In this paper, we introduce a generative latent coding (GLC) scheme for image compression and video compression, referred to as GLC-image and GLC-video, respectively. Unlike most existing pixel-space codecs, GLC-image and GLC-video perform transform coding in the latent space of a generative VQ-VAE, achieving high-fidelity and high-realism generative compression at ultra-low bitrates. Furthermore, compared to VQ-indices-map coding, our approach supports rate-variable compression, a critical feature for practical image and video codecs. GLC-image investigates to code images in the generative latent space and incorporate a spatial categorical hyper module to reduce the bit cost of coding hyper information. GLC-video further verifies the feasibility of coding videos in the generative latent space and proposes a spatio-temporal categorical hyper module to non-uniformly encode the hyper information to improve the performance. To fully leverage the potential of such generative latent coding pipeline, A code-prediction-based supervision is introduced to facilitate the training. Experimental results show that GLC-image and GLC-video achieve higher perceptual quality at much lower bitrates compared to existing generative codecs.

REFERENCES

- [1] G. K. Wallace, "The jpeg still picture compression standard," *Communications of the ACM*, vol. 34, no. 4, pp. 30–44, 1991.
- [2] B. Bross, Y.-K. Wang, Y. Ye, S. Liu, J. Chen, G. J. Sullivan, and J.-R. Ohm, "Overview of the versatile video coding (vvc) standard and its applications," *IEEE Transactions on Circuits and Systems for Video Technology*, vol. 31, no. 10, pp. 3736–3764, 2021.
- [3] J. Ballé, D. Minnen, S. Singh, S. J. Hwang, and N. Johnston, "Variational image compression with a scale hyperprior," in *International Conference on Learning Representations*, 2018.
- [4] Z. Cheng, H. Sun, M. Takeuchi, and J. Katto, "Learned image compression with discretized gaussian mixture likelihoods and attention modules," in *Proceedings of the IEEE/CVF conference on computer vision and pattern recognition*, 2020, pp. 7939–7948.
- [5] Z. Guo, Z. Zhang, R. Feng, and Z. Chen, "Causal contextual prediction for learned image compression," *IEEE Transactions on Circuits and Systems for Video Technology*, vol. 32, no. 4, pp. 2329–2341, 2022.
- [6] W. Guo-Hua, J. Li, B. Li, and Y. Lu, "Evc: Towards real-time neural image compression with mask decay," in *The Eleventh International Conference on Learning Representations*, 2022.
- [7] J. Liu, H. Sun, and J. Katto, "Learned image compression with mixed transformer-cnn architectures," in *Proceedings of the IEEE/CVF Conference on Computer Vision and Pattern Recognition*, 2023, pp. 14 388–14 397.
- [8] Z. Hu, G. Lu, and D. Xu, "Fvc: A new framework towards deep video compression in feature space," in *Proceedings of the IEEE/CVF Conference on Computer Vision and Pattern Recognition*, 2021, pp. 1502–1511.
- [9] J. Li, B. Li, and Y. Lu, "Deep contextual video compression," *Advances in Neural Information Processing Systems*, vol. 34, pp. 18 114–18 125, 2021.
- [10] Y.-H. Chen, H.-S. Xie, C.-W. Chen, Z.-L. Gao, M. Benjak, W.-H. Peng, and J. Ostermann, "Maskcrt: Masked conditional residual transformer for learned video compression," *IEEE Transactions on Circuits and Systems for Video Technology*, vol. 34, no. 11, pp. 11 980–11 992, 2024.

- [11] K. Lin, C. Jia, X. Zhang, S. Wang, S. Ma, and W. Gao, "Dmvc: Decomposed motion modeling for learned video compression," *IEEE Transactions on Circuits and Systems for Video Technology*, vol. 33, no. 7, pp. 3502–3515, 2023.
- [12] J. Ballé, V. Laparra, and E. P. Simoncelli, "End-to-end optimized image compression," in *5th International Conference on Learning Representations, ICLR 2017*, 2017.
- [13] M. J. Muckley, A. El-Nouby, K. Ullrich, H. Jégou, and J. Verbeek, "Improving statistical fidelity for neural image compression with implicit local likelihood models," in *International Conference on Machine Learning*, 2023.
- [14] J. Johnson, A. Alahi, and L. Fei-Fei, "Perceptual losses for real-time style transfer and super-resolution," in *Computer Vision—ECCV 2016: 14th European Conference, Amsterdam, The Netherlands, October 11–14, 2016, Proceedings, Part II 14*. Springer, 2016, pp. 694–711.
- [15] I. Goodfellow, J. Pouget-Abadie, M. Mirza, B. Xu, D. Warde-Farley, S. Ozair, A. Courville, and Y. Bengio, "Generative adversarial nets," *Advances in neural information processing systems*, vol. 27, 2014.
- [16] K. Ding, K. Ma, S. Wang, and E. P. Simoncelli, "Image quality assessment: Unifying structure and texture similarity," *IEEE transactions on pattern analysis and machine intelligence*, vol. 44, no. 5, pp. 2567–2581, 2020.
- [17] A. Van Den Oord, O. Vinyals et al., "Neural discrete representation learning," *Advances in neural information processing systems*, vol. 30, 2017.
- [18] P. Esser, R. Rombach, and B. Ommer, "Taming transformers for high-resolution image synthesis," in *Proceedings of the IEEE/CVF conference on computer vision and pattern recognition*, 2021, pp. 12 873–12 883.
- [19] W. Jiang, H. Choi, and F. Racapé, "Adaptive human-centric video compression for humans and machines," in *Proceedings of the IEEE/CVF Conference on Computer Vision and Pattern Recognition*, 2023, pp. 1121–1129.
- [20] Q. Mao, T. Yang, Y. Zhang, S. Pan, M. Wang, S. Wang, and S. Ma, "Extreme image compression using fine-tuned vqgan models," *arXiv preprint arXiv:2307.08265*, 2023.
- [21] S. Zhou, K. Chan, C. Li, and C. C. Loy, "Towards robust blind face restoration with codebook lookup transformer," *Advances in Neural Information Processing Systems*, vol. 35, pp. 30 599–30 611, 2022.
- [22] G. Toderici, L. Theis, N. Johnston, E. Agustsson, F. Mentzer, J. Ballé, W. Shi, and R. Timofte, "Clic 2020: Challenge on learned image compression, 2020," 2020.
- [23] R. Yang, R. Timofte, and L. Van Gool, "Perceptual learned video compression with recurrent conditional gan," in *IJCAI*, 2022, pp. 1537–1544.
- [24] J. Li, B. Li, and Y. Lu, "Neural video compression with feature modulation," in *IEEE/CVF Conference on Computer Vision and Pattern Recognition, CVPR 2024, Seattle, WA, USA, June 17–21, 2024*, 2024.
- [25] Z. Jia, J. Li, B. Li, H. Li, and Y. Lu, "Generative latent coding for ultra-low bitrate image compression," in *Proceedings of the IEEE/CVF Conference on Computer Vision and Pattern Recognition*, 2024, pp. 26 088–26 098.
- [26] Z. Li, Y. Zhou, H. Wei, C. Ge, and J. Jiang, "Towards extreme image compression with latent feature guidance and diffusion prior," *IEEE Transactions on Circuits and Systems for Video Technology*, vol. PP, pp. 1–1, 01 2024.
- [27] J. Lee, S. Cho, and S.-K. Beack, "Context-adaptive entropy model for end-to-end optimized image compression," in *International Conference on Learning Representations*, 2018.
- [28] J. Li, B. Li, and Y. Lu, "Neural video compression with diverse contexts," in *Proceedings of the IEEE/CVF Conference on Computer Vision and Pattern Recognition*, 2023, pp. 22 616–22 626.
- [29] J. Zhao, B. Li, J. Li, R. Xiong, and Y. Lu, "A universal optimization framework for learning-based image codec," *ACM Transactions on Multimedia Computing, Communications and Applications*, vol. 20, no. 1, pp. 1–19, 2023.
- [30] Z. Cui, J. Wang, S. Gao, T. Guo, Y. Feng, and B. Bai, "Asymmetric gained deep image compression with continuous rate adaptation," in *Proceedings of the IEEE/CVF Conference on Computer Vision and Pattern Recognition*, 2021, pp. 10 532–10 541.
- [31] E. Agustsson, M. Tschannen, F. Mentzer, R. Timofte, and L. V. Gool, "Generative adversarial networks for extreme learned image compression," in *Proceedings of the IEEE/CVF International Conference on Computer Vision*, 2019, pp. 221–231.
- [32] Y. Hu, S. Yang, W. Yang, L.-Y. Duan, and J. Liu, "Towards coding for human and machine vision: A scalable image coding approach," in *2020 IEEE International Conference on Multimedia and Expo (ICME)*. IEEE, 2020, pp. 1–6.
- [33] E. Lei, Y. B. Uslu, H. Hassani, and S. S. Bidokhti, "Text+ sketch: Image compression at ultra low rates," in *ICML 2023 Workshop Neural Compression: From Information Theory to Applications*, 2023.
- [34] F. Mentzer, G. D. Toderici, M. Tschannen, and E. Agustsson, "High-fidelity generative image compression," *Advances in Neural Information Processing Systems*, vol. 33, pp. 11 913–11 924, 2020.
- [35] D. He, Z. Yang, H. Yu, T. Xu, J. Luo, Y. Chen, C. Gao, X. Shi, H. Qin, and Y. Wang, "Po-elic: Perception-oriented efficient learned image coding," in *Proceedings of the IEEE/CVF Conference on Computer Vision and Pattern Recognition*, 2022, pp. 1764–1769.
- [36] E. Hoogeboom, E. Agustsson, F. Mentzer, L. Versari, G. Toderici, and L. Theis, "High-fidelity image compression with score-based generative models," *arXiv preprint arXiv:2305.18231*, 2023.
- [37] S. Iwai, T. Miyazaki, Y. Sugaya, and S. Omachi, "Fidelity-controllable extreme image compression with generative adversarial networks," in *2020 25th International Conference on Pattern Recognition (ICPR)*. IEEE, 2021, pp. 8235–8242.
- [38] E. Agustsson, D. Minnen, G. Toderici, and F. Mentzer, "Multi-realism image compression with a conditional generator," in *Proceedings of the IEEE/CVF Conference on Computer Vision and Pattern Recognition*, 2023, pp. 22 324–22 333.
- [39] F. Gao, X. Deng, J. Jing, X. Zou, and M. Xu, "Extremely low bit-rate image compression via invertible image generation," *IEEE Transactions on Circuits and Systems for Video Technology*, vol. 34, no. 8, pp. 6993–7004, 2024.
- [40] J. Ho, A. Jain, and P. Abbeel, "Denoising diffusion probabilistic models," *Advances in neural information processing systems*, vol. 33, pp. 6840–6851, 2020.
- [41] M. Careil, M. J. Muckley, J. Verbeek, and S. Lathuilière, "Towards image compression with perfect realism at ultra-low bitrates," in *The Twelfth International Conference on Learning Representations*, 2023.
- [42] Z. Wang, E. P. Simoncelli, and A. C. Bovik, "Multiscale structural similarity for image quality assessment," in *The Thirty-Seventh Asilomar Conference on Signals, Systems & Computers*, 2003, vol. 2. Ieee, 2003, pp. 1398–1402.
- [43] G. Lu, W. Ouyang, D. Xu, X. Zhang, C. Cai, and Z. Gao, "Dvc: An end-to-end deep video compression framework," in *Proceedings of the IEEE/CVF Conference on Computer Vision and Pattern Recognition*, 2019, pp. 11 006–11 015.
- [44] G. Lu, X. Zhang, W. Ouyang, L. Chen, Z. Gao, and D. Xu, "An end-to-end learning framework for video compression," *IEEE transactions on pattern analysis and machine intelligence*, vol. 43, no. 10, pp. 3292–3308, 2020.
- [45] Z. Hu, G. Lu, J. Guo, S. Liu, W. Jiang, and D. Xu, "Coarse-to-fine deep video coding with hyperprior-guided mode prediction," in *Proceedings of the IEEE/CVF Conference on Computer Vision and Pattern Recognition*, 2022, pp. 5921–5930.
- [46] W. Ma, J. Li, B. Li, and Y. Lu, "Uncertainty-Aware Deep Video Compression with Ensembles," *IEEE Transactions on Multimedia*, 2024.
- [47] Y.-H. Ho, C.-P. Chang, P.-Y. Chen, A. Gnutti, and W.-H. Peng, "Canfvc: Conditional augmented normalizing flows for video compression," *arXiv preprint arXiv:2207.05315*, 2022.
- [48] L. Qi, J. Li, B. Li, H. Li, and Y. Lu, "Motion information propagation for neural video compression," in *Proceedings of the IEEE/CVF Conference on Computer Vision and Pattern Recognition*, 2023, pp. 6111–6120.
- [49] L. Qi, Z. Jia, J. Li, B. Li, H. Li, and Y. Lu, "Long-term temporal context gathering for neural video compression," in *European Conference on Computer Vision*. Springer, 2024, pp. 305–322.
- [50] X. Sheng, L. Li, D. Liu, and H. Li, "Spatial decomposition and temporal fusion based inter prediction for learned video compression," *IEEE Transactions on Circuits and Systems for Video Technology*, vol. 34, no. 7, pp. 6460–6473, 2024.
- [51] M. Li, Y. Shi, J. Wang, and Y. Huang, "High visual-fidelity learned video compression," in *Proceedings of the 31st ACM International Conference on Multimedia*, 2023, pp. 8057–8066.
- [52] X. Chen, D. P. Kingma, T. Salimans, Y. Duan, P. Dhariwal, J. Schulman, I. Sutskever, and P. Abbeel, "Variational lossy autoencoder," *arXiv preprint arXiv:1611.02731*, 2016.
- [53] A. Van Den Oord, N. Kalchbrenner, and K. Kavukcuoglu, "Pixel recurrent neural networks," in *International conference on machine learning*. PMLR, 2016, pp. 1747–1756.
- [54] R. Rombach, A. Blattmann, D. Lorenz, P. Esser, and B. Ommer, "High-resolution image synthesis with latent diffusion models," in *Proceedings of the IEEE/CVF conference on computer vision and pattern recognition*, 2022, pp. 10 684–10 695.

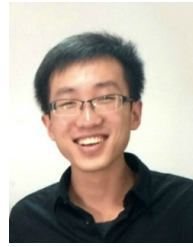
- [55] J. Li, B. Li, and Y. Lu, "Hybrid spatial-temporal entropy modelling for neural video compression," in *Proceedings of the 30th ACM International Conference on Multimedia*, 2022, pp. 1503–1511.
- [56] K. Simonyan and A. Zisserman, "Very deep convolutional networks for large-scale image recognition," *arXiv preprint arXiv:1409.1556*, 2014.
- [57] A. Vaswani, N. Shazeer, N. Parmar, J. Uszkoreit, L. Jones, A. N. Gomez, L. Kaiser, and I. Polosukhin, "Attention is all you need," *Advances in neural information processing systems*, vol. 30, 2017.
- [58] A. Kuznetsova, H. Rom, N. Alldrin, J. Uijlings, I. Krasin, J. Pont-Tuset, S. Kamali, S. Popov, M. Mallocci, A. Kolesnikov et al., "The open images dataset v4: Unified image classification, object detection, and visual relationship detection at scale," *International Journal of Computer Vision*, vol. 128, no. 7, pp. 1956–1981, 2020.
- [59] T. Xue, B. Chen, J. Wu, D. Wei, and W. T. Freeman, "Video enhancement with task-oriented flow," *International Journal of Computer Vision*, vol. 127, no. 8, pp. 1106–1125, 2019.
- [60] I. Loshchilov and F. Hutter, "Fixing weight decay regularization in adam," 2018.
- [61] Kodak Lossless True Color Image Suite, <http://r0k.us/graphics/kodak/>.
- [62] E. Agustsson and R. Timofte, "Ntire 2017 challenge on single image super-resolution: Dataset and study," in *Proceedings of the IEEE conference on computer vision and pattern recognition workshops*, 2017, pp. 126–135.
- [63] T.-Y. Lin, M. Maire, S. Belongie, J. Hays, P. Perona, D. Ramanan, P. Dollár, and C. L. Zitnick, "Microsoft coco: Common objects in context," in *Computer Vision–ECCV 2014: 13th European Conference, Zurich, Switzerland, September 6–12, 2014, Proceedings, Part V 13*. Springer, 2014, pp. 740–755.
- [64] A. Mercat, M. Viitanen, and J. Vanne, "Uvg dataset: 50/120fps 4k sequences for video codec analysis and development," in *Proceedings of the 11th ACM Multimedia Systems Conference*, 2020, pp. 297–302.
- [65] H. Wang, W. Gan, S. Hu, J. Y. Lin, L. Jin, L. Song, P. Wang, I. Katsavounidis, A. Aaron, and C.-C. J. Kuo, "Mcl-jcv: a jnd-based h. 264/avc video quality assessment dataset," in *2016 IEEE international conference on image processing (ICIP)*. IEEE, 2016, pp. 1509–1513.
- [66] G. J. Sullivan, J.-R. Ohm, W.-J. Han, and T. Wiegand, "Overview of the high efficiency video coding (hevc) standard," *IEEE Transactions on circuits and systems for video technology*, vol. 22, no. 12, pp. 1649–1668, 2012.
- [67] M. Heusel, H. Ramsauer, T. Unterthiner, B. Nessler, and S. Hochreiter, "Gans trained by a two time-scale update rule converge to a local nash equilibrium," *Advances in neural information processing systems*, vol. 30, 2017.
- [68] M. Bińkowski, D. J. Sutherland, M. Arbel, and A. Gretton, "Demystifying mmd gans," *arXiv preprint arXiv:1801.01401*, 2018.
- [69] G. Bjontegaard, "Calculation of average psnr differences between rd-curves," *ITU SG16 Doc. VCEG-M33*, 2001.
- [70] L. Van der Maaten and G. Hinton, "Visualizing data using t-sne," *Journal of machine learning research*, vol. 9, no. 11, 2008.
- [71] Z. Yang, J. Teng, W. Zheng, M. Ding, S. Huang, J. Xu, Y. Yang, W. Hong, X. Zhang, G. Feng et al., "Cogvideox: Text-to-video diffusion models with an expert transformer," *arXiv preprint arXiv:2408.06072*, 2024.



Linfeng Qi received the B.S. degree in electronic information engineering from University of Science and Technology of China (USTC), Hefei, Anhui, China, in 2020. He is currently pursuing the Ph.D. degree with the Department of Electronic Engineering and Information Science, USTC. He is also an intern at the Media Computing Group at Microsoft Research Asia. His research interests include video compression and media computing.



Zhaoyang Jia received his B.S. degree in 2022 from the University of Science and Technology of China (USTC). Currently, he is pursuing the Ph.D. degree at the University of Science and Technology of China. He is also an intern at the Media Computing Group at Microsoft Research Asia. His research interests include media compression, media computing and digital watermarking.



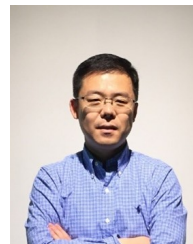
Jiahao Li received the B.S. degree in computer science and technology from the Harbin Institute of Technology in 2014, and the Ph.D. degree from Peking University in 2019. He is currently a Senior Researcher with the Media Computing Group, Microsoft Research Asia. His research interests include neural video compression and other video tasks, like video backbone design and video representation learning. He has more than thirty published papers, standard proposals, and patents in the related area.



Bin Li (Member, IEEE) received the B.S. and Ph.D. degrees in electronic engineering from the University of Science and Technology of China (USTC), Hefei, Anhui, China, in 2008 and 2013, respectively. He joined Microsoft Research Asia (MSRA), Beijing, China, in 2013 and now he is a Principal Researcher. He has authored or co-authored over 50 papers. He holds over 30 granted or pending U.S. patents in the area of image and video coding. He has more than 40 technical proposals that have been adopted by Joint Collaborative Team on Video Coding. His current research interests include video coding, processing, transmission, and communication. Dr. Li received the best paper award for the International Conference on Mobile and Ubiquitous Multimedia from Association for Computing Machinery in 2011. He received the Top 10% Paper Award of 2014 IEEE International Conference on Image Processing. He received the best paper award of IEEE Visual Communications and Image Processing 2017.



Houqiang Li (Fellow, IEEE) received the B.S., M.Eng., and Ph.D. degrees in electronic engineering from the University of Science and Technology of China, Hefei, China, in 1992, 1997, and 2000, respectively. He is a Professor with the Department of Electronic Engineering and Information Science, University of Science and Technology of China. He was a Winner of the National Science Funds (NSFC) for Distinguished Young Scientists, the Distinguished Professor of the Changjiang Scholars Program of China, and the Leading Scientist of the Ten Thousand Talent Program of China. He has authored or coauthored over 200 papers in journals and conferences. His research interests include multimedia search, image/video analysis, video coding, and communication. He was a recipient of the National Technological Invention Award of China (second class) in 2019 and the National Natural Science Award of China (second class) in 2015. He was also a recipient of the Best Paper Award for VCIP 2012, the Best Paper Award for ICIMCS 2012, and the Best Paper Award for ACM MUM in 2011. He served as the TPC Co-Chair for VCIP 2010 and the General Co-Chair for ICME 2021. He served as an Associate Editor for IEEE TRANSACTIONS ON CIRCUITS AND SYSTEMS FOR VIDEO TECHNOLOGY, from 2010 to 2013.



Yan Lu received his Ph.D. degree in computer science from Harbin Institute of Technology, China. He joined Microsoft Research Asia in 2004, where he is now a Partner Research Manager and manages research on media computing and communication. He and his team have transferred many key technologies and research prototypes to Microsoft products. From 2001 to 2004, he was a team lead of video coding group in the JDL Lab, Institute of Computing Technology, China. From 1999 to 2000, he was with the City University of Hong Kong as a research assistant. Yan Lu has broad research interests in the fields of real-time communication, computer vision, video analytics, audio enhancement, virtualization, and mobile-cloud computing. He holds 30+ granted US patents and has published 100+ papers in refereed journals and conference proceedings.